Heliyon 10 (2024) e34789

Contents lists available at ScienceDirect

Heliyon

journal homepage: www.cell.com/heliyon

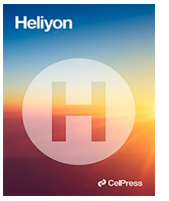

Research article

Preparation of Fe/Co bimetallic oxide loaded hydrophobic & catalytic bifunctional membrane and its catalytic performance in sulfite oxidation

Lijuan Feng [a], Jie Liu [a,b,c,*], Shizhao Wang [a,b,c], Yingying Zhao [a,b,c], Fei Li [a,b,c], Xiaofu Guo [a,b,c], Junsheng Yuan [a,b,c]

[a] School of Chemical Engineering and Technology, Hebei University of Technology, Tianjin, 300130, PR China
[b] Engineering Research Center of Seawater Utilization of Ministry of Education, Tianjin, 300130, PR China
[c] Hebei Collaborative Innovation Center of Modern Marine Chemical Technology, Tianjin, 300130, PR China

ARTICLE INFO

Keywords:
Bimetallic oxides catalyst
CTAB assisted
Desulfurization sulfite wastewater

ABSTRACT

Sulfite oxidation is critical for the stable operation of desulfurization process and the treatment & recovery of desulfurization by-products. The Fe and Co oxides modified super hydrophobic layer was prepared on tubular ceramic membranes using hydrothermal synthesis and surface modifications to realize the combination of the membrane catalysis and membrane aeration. These two oxides were approximately two-layer distributed on the membrane surface, among which the Fe_2O_3 located in the bottom layer and the Co_3O_4 located in the upper layer. The catalytic rate of the bifunctional membrane was about 5.8 times than that of the original ceramic membrane, which was decreased with the increasing of Fe/Co ratio and declined after an initial rise with the increase of urea and cetyltrimethylammonium bromide. The conjoint effect of Fe and Co could improve the catalytic performance and reduce the dissolution loss of catalyzer. The oxidation rate tended to be constant after a 15 % decrease in 7 times experiments.

1. Introduction

SO_2 is an atmospheric contaminant originating from the combustion of fossil fuels and the exhaust of oil refineries. It could directly cause irritation and damage to the respiratory system, and could also be adsorbed on the particulate matter in atmosphere to form haze, or react with water vapor to form acid rain [1,2]. Various desulfurization technologies have been developed to solve the SO_2 pollution problem. Wet desulfurization technology is the most widely applied one [3], including limestone-gypsum desulfurization [4], dual-alkali desulfurization [5], magnesium oxide desulfurization [6], ammonia desulfurization [7] and seawater desulfurization [8]. As an unstable pollutant, the sulfite generated in desulfurization wastewater is likely to release SO_2, causing air and water contamination. There are normally two kinds of methods for the treatment of sulfite. The first one is the inhibition of the oxidation applied in the magnesium desulfurization process, in which magnesium sulfite is calcined into magnesium oxide as a product [9]. The most widely applied one is the promotion of oxidation to obtain more stable sulfate [10].

The transition metals have been proved to be the efficient catalysts in many oxidation reactions, among which supported bimetallic oxides catalyst have drawn a lot of attention. It presents outstanding synergistic catalytic effect with greater numbers of activated

* Corresponding author. School of Chemical Engineering and Technology, Hebei University of Technology, Tianjin, 300130, PR China.
E-mail address: liujie@hebut.edu.cn (J. Liu).

https://doi.org/10.1016/j.heliyon.2024.e34789
Received 26 January 2024; Received in revised form 27 June 2024; Accepted 17 July 2024
Available online 18 July 2024

Table 1
Parameters of the ceramic membrane tube.

pore size (nm)	material	length (mm)	inner and outer diameter (mm)	porosity
200	ZrO_2, Al_2O_3	50	8, 10	30–35 %

oxygen species, higher electron transfer efficiency and easier adsorption of reactants [11]. Activated carbon [12], molecular sieves [13], and ceramic membranes [10] are the most used supports. Liu et al. [12] reported that the catalyst prepared with Co and Mn could enhance the dispersion of mixed oxides, and the presence of Mn species could help to promote the generation of surface-adsorbed oxygen, which was benefit to sulfite oxidation. Sun et al. [14] prepared Co–Fe layered double oxide catalyst with different atomic ratios. It exhibited a removal ratio of carbamazepine higher than 99 % in 30 min in the degradation process, which would be caused by the specific structure of the layered double oxide and the synergistic effect of Co, Fe, and Al. Zhang et al. [15] prepared Fe/Co-based sulfide nanocomposite catalysts, where Co and Fe enhanced the binding state of intermediates containing oxygen at the Co/Fe active site, and increased catalytic activity.

As the oxidation of sulfite is a gas-liquid reaction, the dispersion of gas in the liquid phase is also important for the mass transfer and the reaction rate. The microporous membranes dispersion is an efficient way [16,17], which has shown promising prospect in biological wastewater treatment [18], CO_2 capture [19] and natural gas sweetening [20], due to the advantage of energy conservation, controllability, and high efficiency. Zhi et al. [16] applied membrane aeration to the electro-Fenton process, the oxygen concentration of which was 2.421 times than that using normal plastic tube ventilation taking only 1/12 of the time. Li et al. [21] used micro-hydrogen bubbles generated by ceramic membranes to facilitate phenol conversion and cyclohexanone uptake in the liquid-phase hydrogenation process of phenol. It was discovered that micro gas bubbles in the reactor caused by membrane feeding might mitigate catalyst deactivation.

The ceramic microporous membranes with excellent chemical stability, thermal stability and mechanical stability can adapt to diverse application environments as efficient catalyst supports. Its abundant porous structure could improve the catalytic performance by providing large specific surface area and more catalytic sites. It could also provide the possibility of combining membrane dispersion and membrane catalysis. Furthermore, unlike the other supports, the ceramic membrane support ensures exceptional stability for catalytic oxidation reactions [22]. In our previous work [10], sea urchins-like MnO_2 particles were prepared on ceramic membrane to fabricate the dispersion & catalysis bifunctional membrane. The oxidation rate of sulfite was increased by 44.0 % in Na_2SO_3 solution and 64.2 % in $(NH_4)_2SO_3$ solution. Meanwhile, the super hydrophobic surface with a maximum static water contact angle of 164.9° was also obtained due to the three-dimensional structure of MnO_2. The hydrophobic surface has been proved to improve the mass transfer of oxygen [23].

Co is a great effective catalytic species for sulfite oxidation. However, the high price and environmental toxicity are its main issues. Although Fe has lower catalytic activity than Co for sulfites, it has a lower price and larger reserves, which makes it more economical and promising for application. More important, some studies have revealed that Fe/Co mixed oxide catalysts can improve the catalytic performance of the catalyst, in which Fe plays a crucial role. Therefore, Fe/Co bimetal oxide catalyst was prepared on a tubular ceramic membrane by the introducing of Fe in this work. Its sulfite oxidation performance in a membrane dispersion & membrane catalysis process was investigated. The effects of calcination temperature, urea dosage, and CTAB dosage on the characteristics and catalytic oxidation performance of the samples were examined.

2. Experiment

2.1. Material and reagents

The tubular ceramic membrane (Table 1) was purchased from Jiangsu Jiuwu Hi-Tech Co., Ltd., China. Cobalt nitrate hexahydrate ($Co(NO_3)_2{\cdot}6H_2O$, 99.99 %) was purchased from Shanghai Aladdin Chemical Co., Ltd., China. Iron nitrate nonahydrate ($Fe(NO_3)_3{\cdot}9H_2O$, 98.5 %), cetyltrimethylammonium bromide ($C_{19}H_{42}BrN$, 99.0 %), urea (CH_4N_2O, 99.0 %) and stearic acid ($C_{18}H_{36}O_2$, 99.7 %) were obtained from Tianjin Kemiou Chemical Reagent Co., Ltd., China. Sodium sulfite anhydrous (Na_2SO_3, 98.0 %) was purchased from Shanghai Macklin Biochemical Co., Ltd., China. All the chemical reagents were analytical grade (AR) and used without any further refinement.

2.2. Preparation

The Fe/Co oxides layer on the ceramic membrane was prepared by hydrothermal method. At first, the original tubular ceramic membrane (CM) was cleaned with ultrasonic in ethanol and distilled water for 10 min, respectively. 5 mmol urea and 0.04 g CTAB were dissolved in 50 mL deionized water. Then 2.5 mmol $Fe(NO_3)_3{\cdot}9H_2O$ and 2.5 mmol $Co(NO_3)_2{\cdot}6H_2O$ were added and stirred vigorously at room temperature for 30 min. The mixed solution was transferred into an 80 mL Teflon-lined stainless-steel autoclave with a vertical 5 cm tubular ceramic membrane and maintained at 140 °C for 12 h. Afterwards, the membrane was washed with ethanol and water alternately, and dried at 60 °C for 1 h. Then, the membrane was calcined at 400 °C for 2 h in a muffle furnace. The obtained sample was named Fe/Co-CM. Finally, the superhydrophobic composite membrane loaded with Fe/Co oxides (SA-Fe/Co-CM) was obtained by soaking the Fe/Co-CM membrane in a 10 mmol/L stearic acid anhydrous ethanol solution for 5 h. The process was

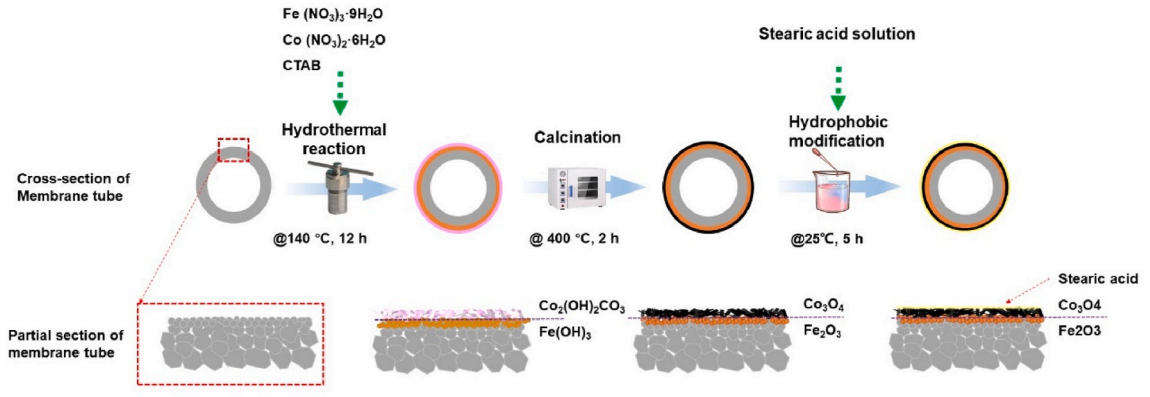

Fig. 1. Preparation process of transition metal modified ceramic membrane.

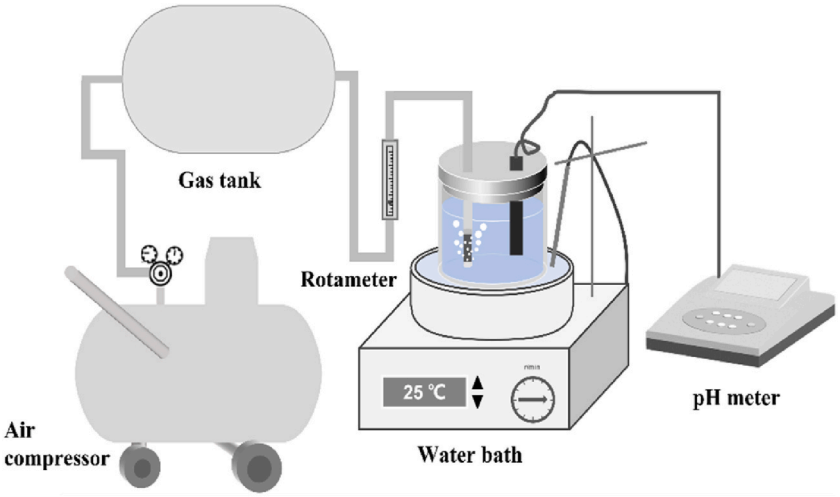

Fig. 2. Schematic diagram of experimental setup for sulfite oxidation.

illustrated in Fig. 1.

The reactions occurred in the hydrothermal process and calcination treatment were shown in Eqs. (1)–(7) [24,25] :

$$CO(NH_2)_2 + 3H_2O \rightarrow 2NH_3 \cdot H_2O + CO_2 \quad (1)$$

$$2NH_3 \cdot H_2O + CO_2 \rightarrow 2NH_4^+ + CO_3^{2-} \quad (2)$$

$$NH_3 \cdot H_2O \rightarrow NH_4^+ + OH^- \quad (3)$$

$$2Co^{2+} + 2OH^- + CO_3^{2-} \rightarrow Co_2(OH)_2CO_3 \quad (4)$$

$$Fe^{3+} + 3OH^- \rightarrow Fe(OH)_3 \quad (5)$$

$$3Co_2(OH)_2CO_3 + O_2 \xrightarrow{\text{calcination}} 2Co_3O_4 + 3H_2O + 3CO_2 \quad (6)$$

$$2Fe(OH)_3 \xrightarrow{\text{calcination}} Fe_2O_3 + 3H_2O \quad (7)$$

2.3. Characterization

The crystal structure was examined by X-ray diffraction (XRD, D8 FOCUS, Bruker Corporation, Germany) with Cu *Kα* radiation (λ = 1.5418 Å). The results were collected between 10° and 70°at a step size of 0.01° and scanning speed of 6°/min. The morphological and elements analysis was performed using a FESEM and EDS (Quanta 450 FEG and Octane Plus, FEI Company, USA), with an accelerating

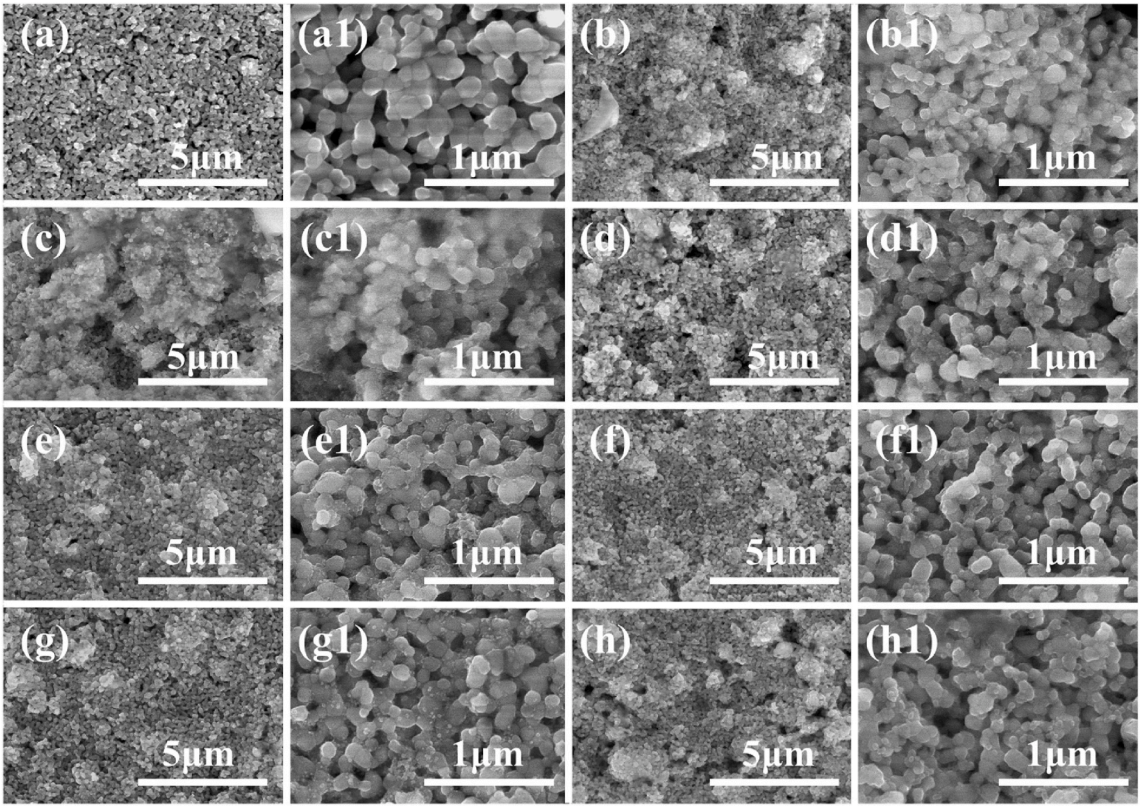

Fig. 3. Surface SEM images of the original membrane: (a, a1) and modified membranes prepared with different Fe/Co ratios: (b, b1) 0:1; (c, c1) 1:3; (d, d1) 1:2; (e, e1) 1:1; (f, f1) 2:1; (g, g1) 3:1; (h, h1) 1:0.

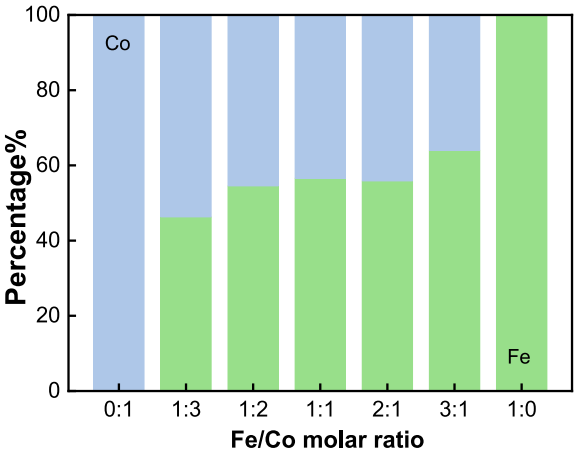

Fig. 4. Percentage of elements on the surface of the modified membranes.

voltage of 20 kV. The chemical composition of samples was analyzed using X-ray photoelectron spectroscopy (XPS) (ESCALAB 250Xi, Thermo Fisher Scientific, USA) with an Al *Kα* source. Flourier transformed infrared (FTIR) spectroscopy was collected on Bruker V80 with a scanning range of 400–4000 cm^{-1}. Raman spectra were collected on an in Via Reflex Renishaw (Renishaw, UK), and the wavelength of laser was 532 nm. Water contact angle (WCA) was examined on Krüss DSA 100 (Krüss Company, Ltd., Germany) using the pendant drop method. The volume of water droplets was 3 μl. The concentration of Fe^{2+} and Co^{3+} dissolved in the sulfite solution was detected by Inductively coupled plasma spectrometer (ICP) (Optima 8300, PE Company, USA).

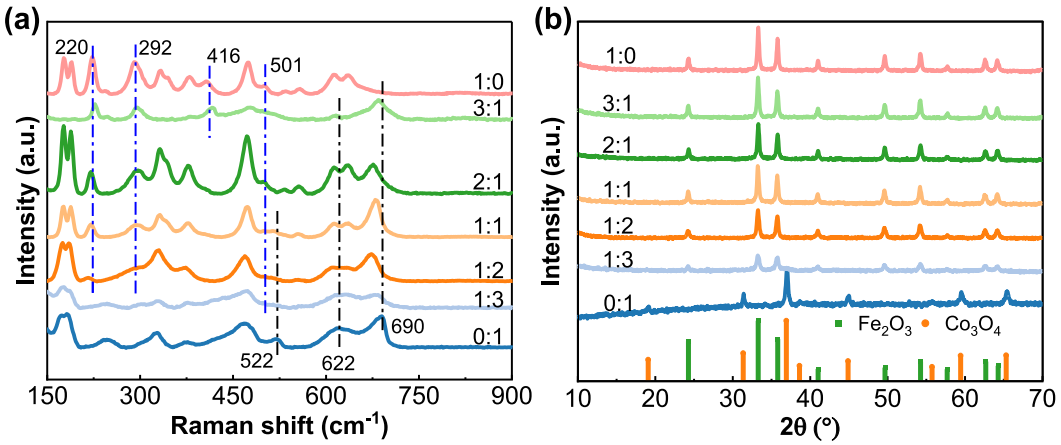

Fig. 5. Prepared with different Fe/Co ratios: (a) Raman spectra of the modified membranes; (b) XRD spectra of powders.

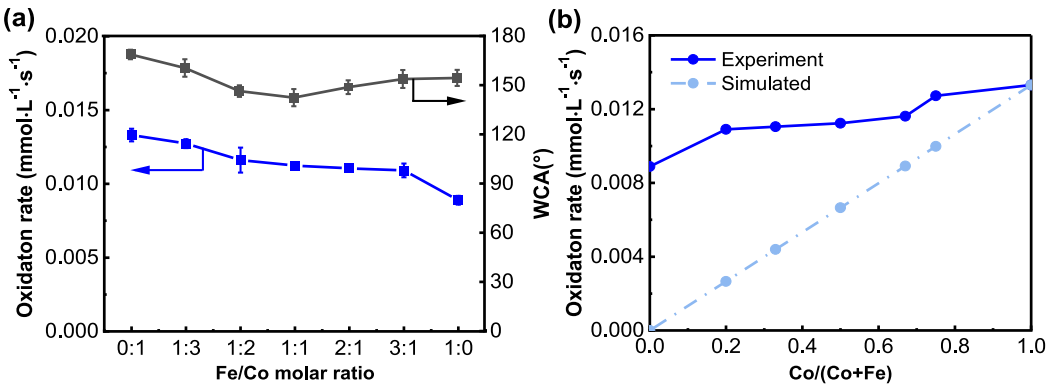

Fig. 6. (a) Water contact angle and catalytic performance of the modified membranes prepared with different Fe/Co ratios; (b) Changes of simulated and experimental values of sodium sulfite oxidation rate with Co percentage.

2.4. Catalytic performance test

The catalytic performance of the membrane in the sulfite oxidation process was evaluated by a membrane dispersion & catalysis apparatus (Fig. 2). The reaction tank with 0.5 L sulfite solution of 50 mmol/L was maintained at 25 °C in a thermostatic water bath. The air was fed into the reactor under a flowrate of 400 ml/min and dispersed by the membrane. The experiment was run 1 h, and the sample was taken every 20 min, the sulfite concentration (C_s) of which was determined using the iodimetry method [26]. During the experiment time, the speed of sulfite oxidation was a nearly constant value over time. Therefore, the oxidation rate of sulfite could be obtained from the slope of the C_s−time curve.

3. Results and discussions

3.1. Effect of Fe/Co ratio

The surface morphology of membranes was shown in Fig. 3. The original membrane was composed of smooth particles forming flat and porous surface, while the surface and pore of the modified membrane was loaded with tightly connected Fe/Co oxide particles as shown in Fig. 3 (a). The space between Fe/Co oxide particles were increased with the decrease of Fe/Co ratio. The Fe and Co contents on the membrane surface shown in Fig. 4 were also indicated that the actual loaded Fe/Co ratios were slightly increased.

The Raman spectra shown in Fig. 5 (a) suggested that Fe_2O_3 and Co_3O_4 were successfully fabricated on the modified membrane surface. Four feature peaks of crystalline Fe_2O_3 at 220, 292, 416 and 501 cm^{-1} were detected in the modified membrane with Fe/Co = 1:0, which would typically be assigned to the A_{1g}, E_g, E_g and A_{1g} modes, respectively [27]. Three feature peaks at 522, 622 and 690 cm^{-1} of crystalline Co_3O_4 were observed in the modified membrane with Fe/Co = 0:1, which would typically be attributed to the F_{2g}, F_{2g} and A_{1g} modes, respectively [28]. As the Fe/Co ratio decreases, the peaks at 522 cm^{-1} and 622 cm^{-1} were gradually weaken and eventually disappeared due to the decrease of loaded Co_3O_4. Additionally, the peaks at 690 cm^{-1} shifts towards the lower wave

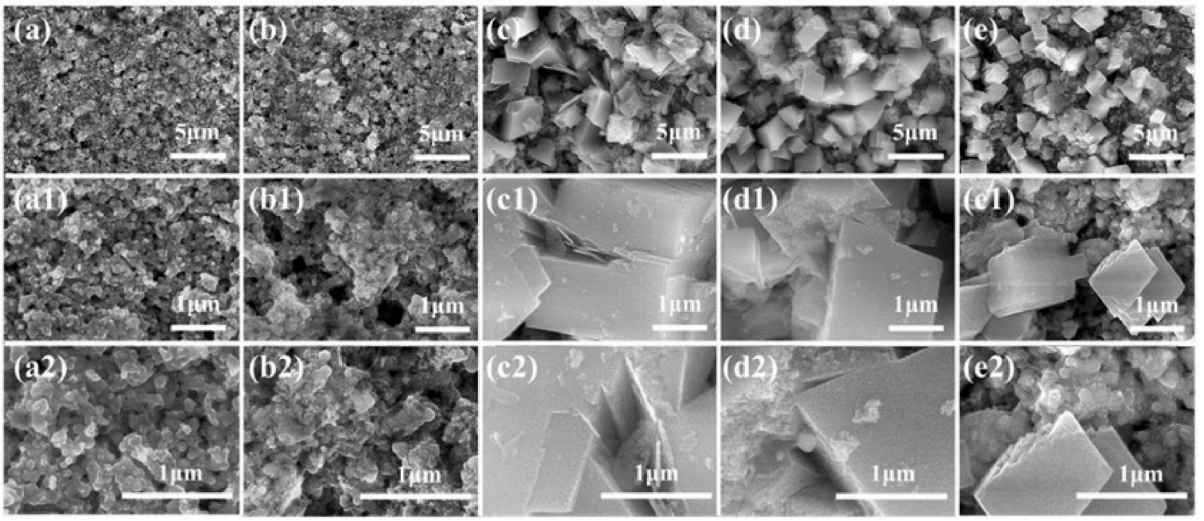

Fig. 7. Surface SEM images of the modified membranes prepared with different nitrate/urea molar ratios: (a, a1, a2) 1:0.5, (b, b1, b2) 1:1, (c, c1, c2) 1:1.5, (d, d1, d2) 1:2, (e, e1, e2) 1:4.

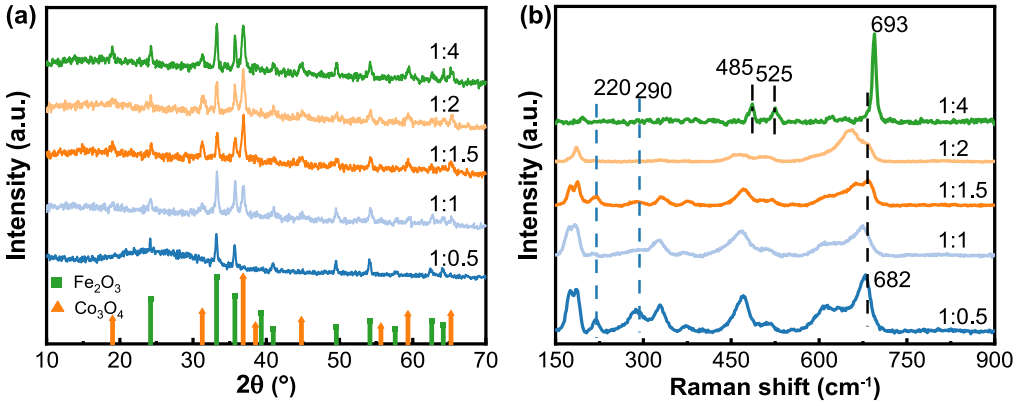

Fig. 8. Prepared with different urea dosages: (a) XRD patterns of powders, (b) Raman spectra of the modified membranes.

number because the interaction between Fe and Co would reduce the Co_3O_4 grain size [29].

The powder obtained during the hydrothermal reaction were tested by XRD, and the results were shown in Fig. 5 (b). The peaks at 33.2° and 35.7° were corresponded to the (121) and (110) lattice planes of α- Fe_2O_3 (JCPDS 89–0599) with R-3c (167) space group hexagonal structures. The intensity of these two characteristic peaks of Fe_2O_3 were increased with the decrease of Fe/Co ratio, indicating an increase of crystallinity. The diffraction peak at 36.8° corresponded to the (311) crystal plane of Co_3O_4 (JCPDS 73–1701) with the Fd-3m (227) space group cubic structure. This diffraction peak with lower intensity could only be observed when the Fe/Co ratio was larger than 1:3. The hydrolysis of urea could supply OH^- to react with metal ions during the hydrothermal process. The molar ratio of nitrate/urea was 1:0.5, and the reaction equilibrium constant of Fe^{3+} and OH^- was higher than that of Co^{2+} and OH^- (log K_{xy} of −18.8 for Co $(OH)_2(aq)$ and −13.1 for Fe $(OH)_3(aq)$) [30]. Therefore, Fe precursors were much easier generated. As a result, there was more Fe_2O_3 than Co_3O_4 which induce to weak intensity of Co_3O_4 peak.

The static water contact angle and catalytic performances were shown in Fig. 6 (a). Most of the contact angles were larger than 150° indicating the obtaining of superhydrophobic surface. The catalytic performance of the modified membranes with various Fe/Co ratios was shown in Fig. 6 (a). The oxidation rate of Na_2SO_3 catalyzed by the membrane loaded with Fe was 0.00889 mmol L^{-1} s^{-1}, while the value using Co was 0.01331 mmol L^{-1} s^{-1}. The catalytic effect of the modified membranes was gradually decreased following with the increase of Fe/Co ratio. It was demonstrated that the catalytic activity of Co was higher and played a more significant role in the reaction. The experimental and simulated values of the Na_2SO_3 oxidation rates catalyzed by modified membranes were shown in Fig. 6 (b). The Na_2SO_3 oxidation rate of the modified membrane loaded with Fe was ignored, and the rate catalyzed by the modified membrane loaded with Co was used as reference [12]. A straight line derived from the points (x = 0, y = 0) and (x = 1, y = 0.01331) could be used to determine the simulated values of the oxidation rate at various Co occupancy ratios. The experimental rates of Na_2SO_3

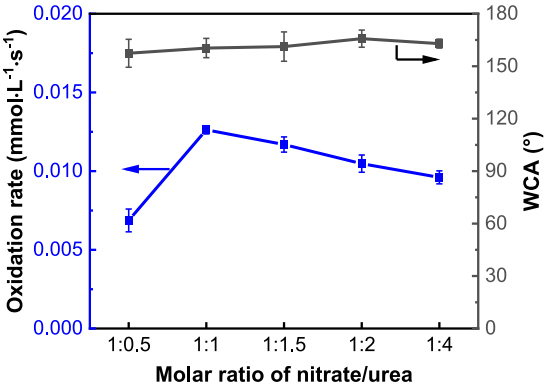

Fig. 9. Effect on the oxidation rate and water contact angle of the modified membranes prepared with different urea dosages.

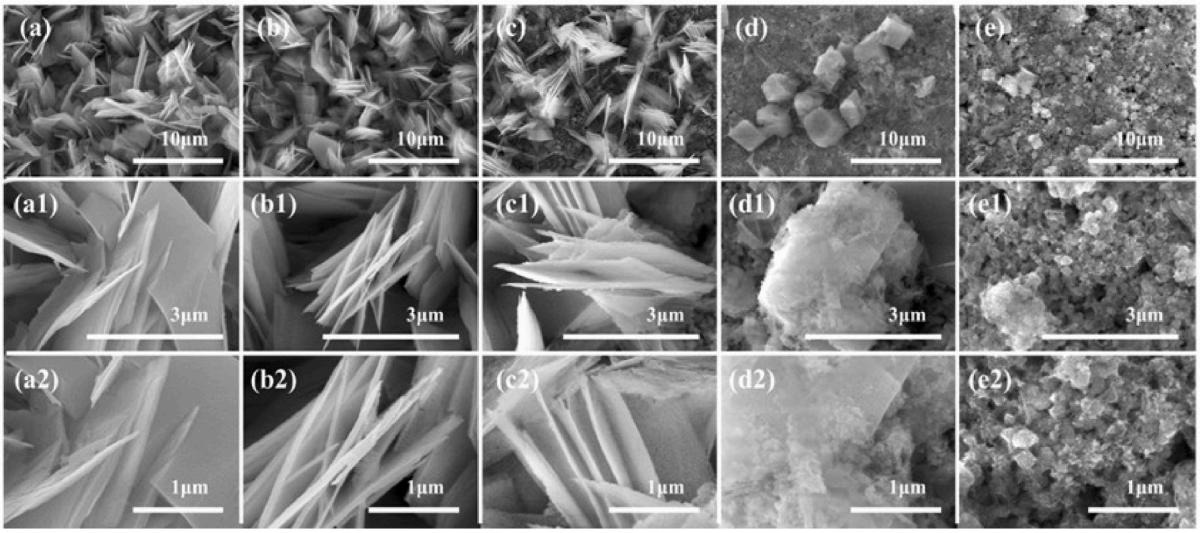

Fig. 10. Surface SEM images of the modified membranes prepared with different CTAB concentration: (a, a1, a2) 0 mmol/L; (b, b1, b2) 1.1 mmol/L; (c, c1, c2) 2.2 mmol/L; (d, d1, d2) 3.3 mmol/L; (e, e1, e2) 4.4 mmol/L.

oxidation catalyzed by bimetallic modified membranes were higher than the simulated value from straight line, which was indicated that there was a synergistic interaction between Co and Fe and that the bimetallic environment was benefit for the catalytic oxidation of Na_2SO_3 by Fe.

3.2. *Effect of urea concentration*

The surface morphology of the modified membrane prepared with different urea concentration was shown in Fig. 7. The amounts of loaded particles were increased with the increase of urea concentration, leading to the formation of large clumps on the membrane surface as shown in Fig. 7 (a2, b2). The large cubic particles composed of sheet-like structures began to be formed on the membrane surface when the mole ratio of nitrate/urea was 1:1.5. As the ratio of nitrate/urea decreased, the amount of sheet-like structure was decreased. The presence of the big particles was caused by the growth-directing of CTAB and the increasing quantity of precipitate as urea concentrations rose. Urea was decomposed in aqueous solutions at temperatures above 80 °C, slowly and steadily supplying OH^- to the reaction system [31]. Therefore, there were more Co oxide generated at higher urea concentrations.

The XRD patterns shown in Fig. 8 (a) indicated that Fe_2O_3 could be observed in each sample, while the diffraction peak at 36.8° of Co_3O_4 could only be considerably observed in the 1:1 pattern, which became higher and sharper as the addition of urea continues to increase. The Raman spectra in Fig. 8 (b) presented that the intensity of the peak related to the bonds of ZrO_2 and Fe_2O_3 were gradually weaken until they were disappeared as the amount of urea increased. The peaks intensity of bonds related to Co_3O_4 were strengthened, indicating that the modified membrane surface is gradually covered by Co_3O_4. Meanwhile, the peak at 682 cm^{-1} was shifted to 693 cm^{-1} and intensified, showing that the sample has a superior spinel structure and better crystalline characteristics [32].

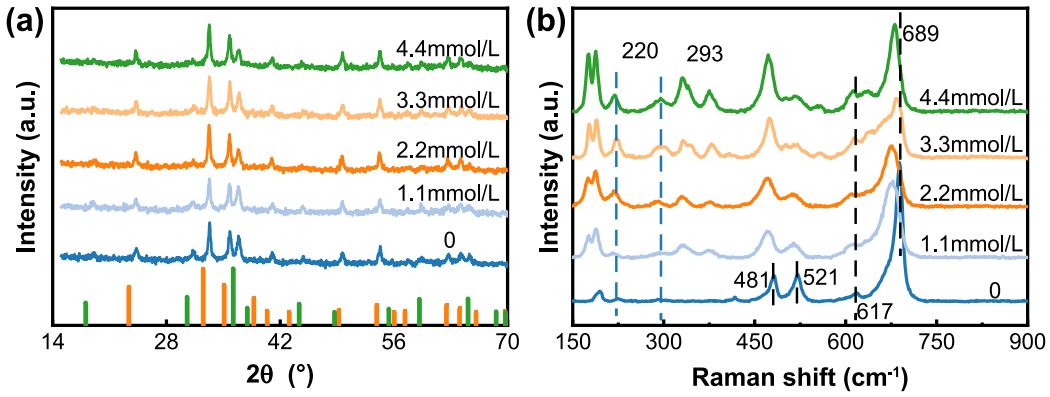

Fig. 11. Prepared with different CTAB concentration: (a) XRD patterns of powders; (b) Raman spectra of the modified membranes.

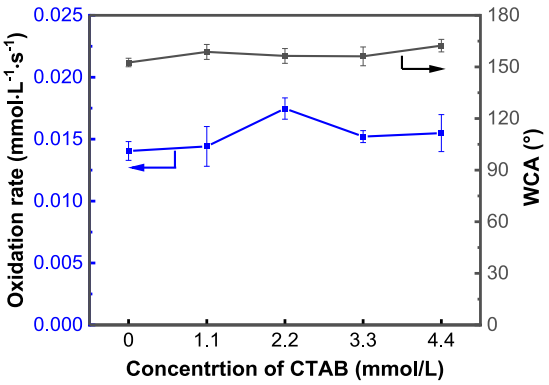

Fig. 12. Water contact angle and catalytic performance of the modified membranes prepared with different CTAB concentration.

The contact angle and catalytic performance shown in Fig. 9 indicated that the contact angle was increased with the increase of urea due to the formation of uniform and dense cubic particles on the surface of the membranes at high urea addition. The catalytic performance was increased when the nitrate/urea ratio decreased from 1:0.5 to 1:1. Then the catalytic performance started to decrease. This was because high concentration of urea would lead to large amount of oxide loaded on the membrane surface, which would block the membrane pores and reduce the specific surface area of the catalyst, reducing the exposure of active site. When the ratio of nitrate/urea amount was 1:1, the modified membrane surface was loaded with enough Co_3O_4 to promote the oxidation of Na_2SO_3.

3.3. *Effect of surfactant concentration*

The surface morphology of the modified membranes prepared at different CTAB concentration was shown in Fig. 10. The surface of the modified membrane prepared without CTAB was covered by many randomly arranged flakes (Fig. 10 a). The positive surfactant ions hydrolyzed from CTAB were existed as particular micelles and could promote metal ions and hydroxide ions to form precipitates. The restriction effect of micelles to the crystal formation could realize the crystal orientation growth [33–35]. Therefore, the more homogeneous and regular shape with higher the specific surface area was formed by the intersected flakes when CTAB was added, as shown in Fig. 10 (b). Then the surfactant ions gathered and formed bigger micelles as the CTAB concentration rose, which was difficult to load on the membrane, so only thin flakes and less irregular thick blocks were able to grow onto the membrane consequently [36]. It was also shown in Fig. 10 that large cubic particles and separate flakes were formed on the membrane surface prepared with larger concentration of CTAB, and only small particles remained on the membrane surface at the highest CTAB concentration.

The diffraction peaks of α-Fe_2O_3 and Co_3O_4 were appeared in the XRD, and the addition of CTAB did not affect the crystalline phases of Fe_2O_3 and Co_3O_4 as shown in Fig. 11 (a). The Raman spectra of the modified membrane were shown in Fig. 11 (b). The intensity of the peaks associated with Fe_2O_3 and ZrO_2 were gradually enhanced, while the ones of Co_3O_4 at 481 cm^{-1} and 521 cm^{-1} were gradually diminished. It was indicated that the Co_3O_4 content on the membrane was reduced, which was consistent with the SEM results. The addition of CTAB shifted the peak of Co_3O_4 located at 689 cm^{-1} to a lower wave number to 676 cm^{-1} (CTAB 2.2 mmol/L).

The contact angle and catalytic oxidation rate were shown in Fig. 12. The contact angle showed slight increase with the increase of

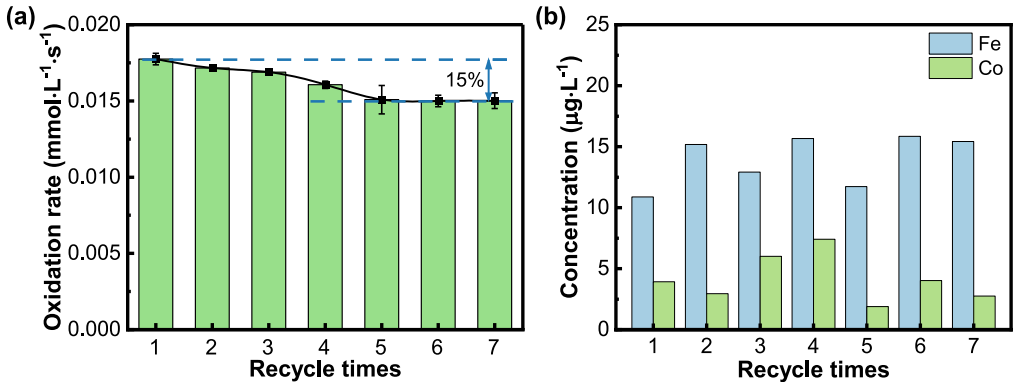

Fig. 13. (a) Oxidation rate of sulfite in different recycle times, (b) Content of Fe^{3+} and Co^{2+} in sulfite solution.

CTAB. The catalytic reaction rate was increased with the addition of CTAB, and reached the maximum value at the point of 2.2 mmol/L. Then reaction rate started to decrease with the increase of CTAB concentration. One reason for this result was that the more CTAB was introduced, the less catalyst was loaded on the membrane surface as revealed by the XRD and Raman analysis. On the other hand, the morphology of catalysts with a small amount of CTAB added is more consistent than that without CTAB, which would lead to a greater specific surface area and more exposure of catalytic sites, thereby higher oxidation rate of sulfite. However, further increasing CTAB would induce to a decrease in the specific surface area of big particles as well as less loading amount on the membrane, resulting in a decrease in the catalytic reaction rate.

3.4. Stability of the modified membrane

The stability of the catalyst is an important character in its application. As can be seen in Fig. 13 (a), the reaction rate of Na_2SO_3 dropped from 0.01774 mmol L^{-1} s^{-1} to 0.01501 mmol L^{-1} s^{-1} after five times experiments, and then kept constant. There would be two possible factors leading to this reduce: the dissolution loss of catalyst and the change of physical & chemical properties of the surface. In terms of catalyst dissolution loss, the concentration of Co^{2+} and Fe^{3+} in the solution after experiments (Fig. 13 (b)) indicated that Fe^{3+} were more unstable and much easier to leached. The XPS spectrum of the modified membrane shown in Fig. 14 (a) were also indicated the more leaching amount of Fe during the reaction. As presented in Table 2, the Fe/Co ratio on the fresh modified membrane surface was 0.7, while the value of the used composite membrane was increased to 0.85.

In terms of physical & chemical properties, the high-resolution spectrogram of main element was shown in Fig. 14 (b). The binding energies of Co $2p_{3/2}$ and Co $2p_{1/2}$ in the Co 2p spectra were changed from 780.26 eV to 780 eV and from 795.11 eV to 795.07 eV after being used. Co $2p_{3/2}$ was fitted to two peaks with binding energies at 779.7 eV for Co^{2+} and 781.0 eV for Co^{3+} [37,38]. The Co^{3+}/Co^{2+} ratios of the samples was increased from 0.65 to 0.89 after being used, which induced to the shift of the Co 2p peak to a lower binding energy [39]. Co^{2+} is the main active species in sulfite catalytic oxidation [40], so the decrease of Co^{2+} would induce to the decrease of catalytic effect of the modified membrane after several experiments. It can be seen from Fig. 14 (c) that $Fe2p_{3/2}$ was fitted to two Fe^{3+}peaks [38,41], both of which were not significant changed after the reaction. From Fig. 14 (e), the O 1s spectrum was further decomposed into three peaks, the one at 529.9 eV corresponding to metal lattice oxygen bonding (M − O), the one at 531.4 eV corresponding to OH, and the third one at 532.9 eV corresponding to surface-bound water (H–*O*–H) [37].

Additionally, as shown in Fig. 14 (d), the one located at 284.7 eV corresponded to the C–C, and C–H in the carbon chain of stearic acid, the one at 285.9 eV corresponded to the carbon atom in the carboxyl group and 288.1 eV was attributed to the signal generated by the combination of metal and carboxyl group [42]. The percentage of such carbon were reduced from 75.33 % to 59.58 % after reaction. Therefore, it could be inferred that the shed of long aliphatic chain of stearic acid and the induced decrease of contact angle was a main reason for the reduced catalytic effect after several tests. From the results of the valence of Fe and Co, the combination mode of C and O, and the changes during the experiment, it could be inferred that the formation of the Fe/Co complex and the reduction of catalytic activity were due to the shedding of hydrophobic substances.

To further analyze the advantages of layered growth of Fe_2O_3 and Co_3O_4 on the membranes, modified membranes loaded with single metal oxides were prepared with 0.05 mol/L iron nitrate and 0.05 mol/L cobalt nitrate, respectively. As shown in Table 3, the catalytic performance of the membrane loaded with bimetallic oxides (SA-Fe/Co-CM) was much higher than that of the membranes loaded with single metal oxide (SA-Co-CM), indicating that the simultaneous growth of Fe/Co on the membrane improved the performance of the catalytic layer. The dissolution loss rates of Co^{2+} and Fe^{3+} were 7.15 ‰ and 2.42 ‰, respectively, which were 2 times of the value of SA-Fe/Co-CM. It was demonstrated that the intermediate layer of Fe_2O_3 can reduce the dissolution loss of Co.

3.5. Performance analysis of the modified membrane

The bifunctional membranes were prepared by catalyst loading and surface modification to improve the catalytic performance.

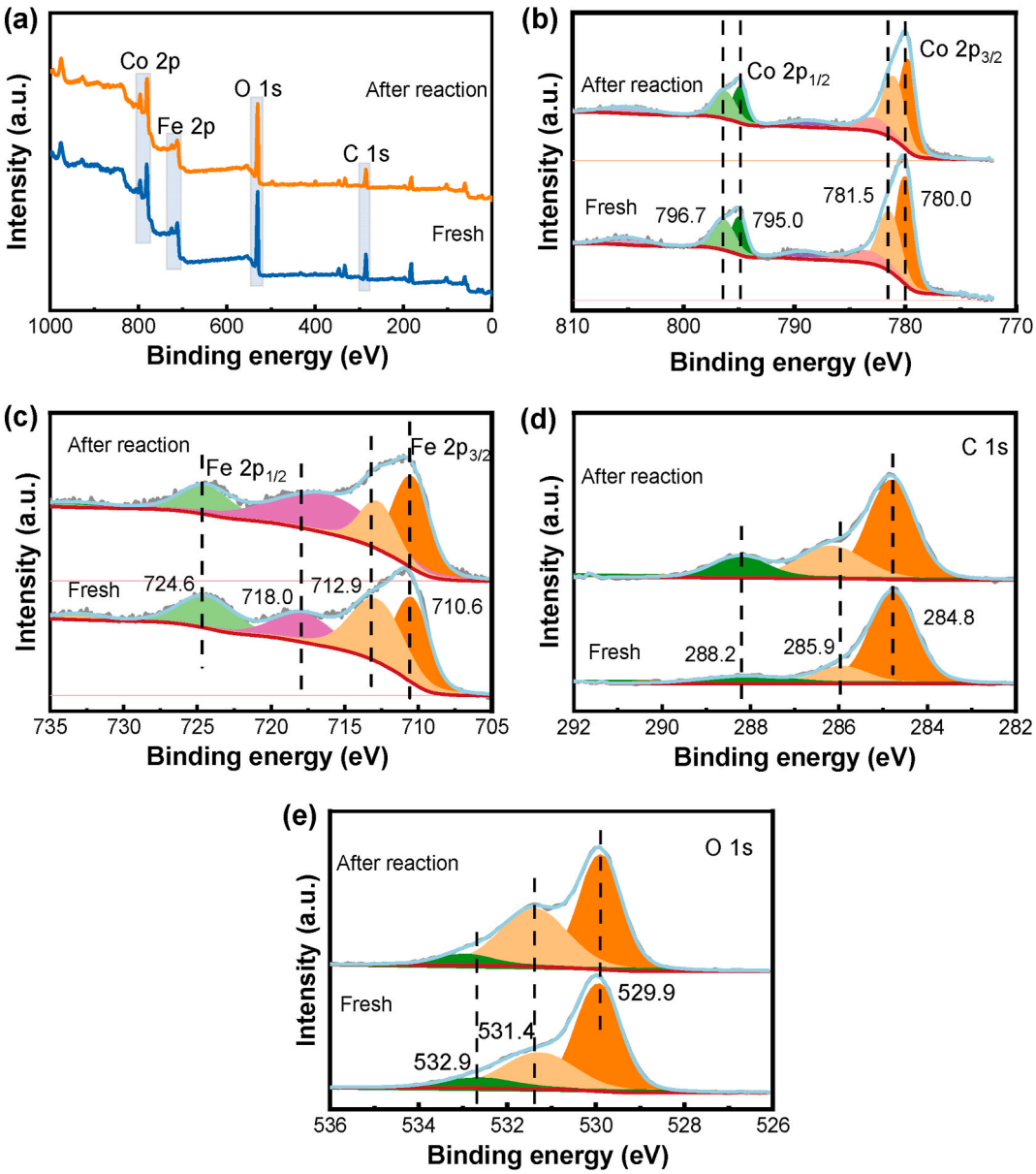

Fig. 14. XPS spectra of modified membranes before and after experiment: (a) wide scan spectrum, (b) Co 2p, (c) Fe 2p, (d) C 1s, and (e) O 1s.

Table 2
Composition variation of membrane before and after used.

Element	Atonic %	
	fresh	used
Co	6.2	6.46
Fe	8.82	7.64
O	45.98	49.65
Zr	2.46	1.69
C	36.54	34.56

Therefore, the roles of Fe oxide, Co oxide, and stearic acid in the membrane properties and catalyst performances were investigated and discussed.

The surface and cross-sectional morphological structures of the membranes were tested and shown in Fig. 15. The surface of the CM membrane was porous structure consisted of smooth particle (Fig. 15 (a)) and has an asymmetric cross-sectional structure (Fig. 15 (c)),

Table 3
Actual metal loading on the membranes and mass fraction of dissolution.

Membrane type	Oxidation rate of sulfite	Loading content (mg)		Metal dissolution (wt.‰)	
	($mmol•L^{-1}•s^{-1}$)	Co	Fe	Co^{2+}	Fe^{3+}
SA-Fe/Co-CM	0.01774	3.179	2.266	1.16	3.40
SA-Co-CM	0.00716	4.914	–	7.15	–
SA-Fe-CM	0.00482	–	2.242	–	2.42

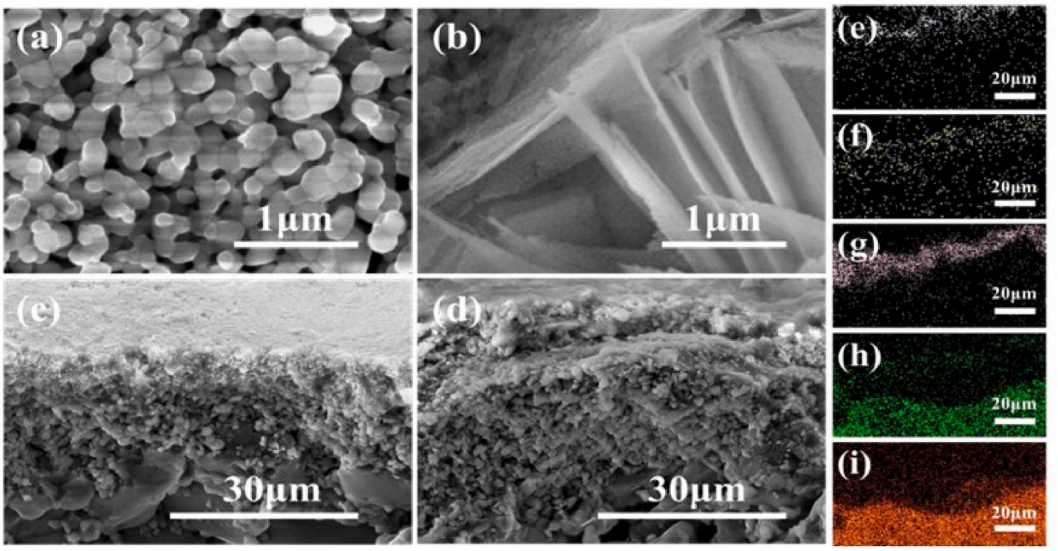

Fig. 15. Surface SEM images of CM: (a) and SA-Fe/Co-CM: (b); Cross section SEM images of CM: (c) and SA-Fe/Co-CM: (d); Elemental mapping images of cross section of SA-Fe/Co-CM, (e) Co; (f) Fe; (g) Zr; (h) Al; (i) O.

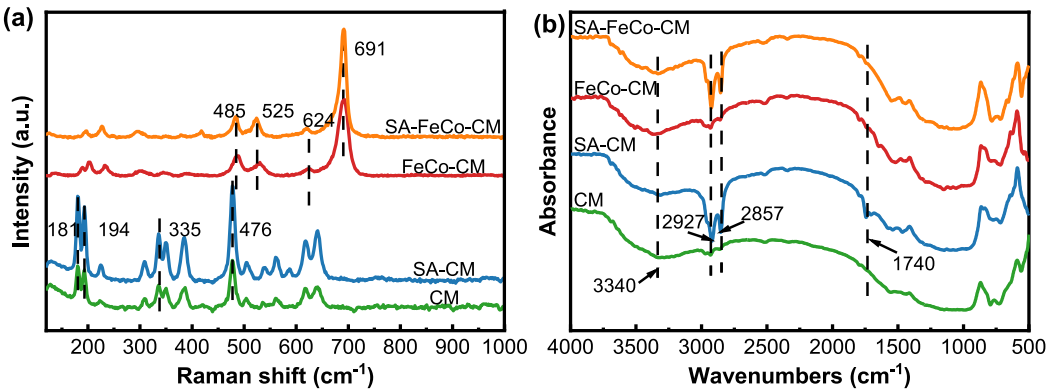

Fig. 16. (a) Raman spectra, (b) FTIR spectra of CM, SA-CM, Fe/Co-CM, and SA-Fe/Co-CM.

consisting of a large particle support layer, an intermediate transition layer and a top dense separation layer. The microstructure of the membrane surface changed into three-dimensional structure of interspersed lamellae corresponding to Co_3O_4 after loaded by catalyst (Fig. 15(b–d)). The elemental distribution of the SA-Fe/Co-CM membrane's cross-section shown in Fig. 15(e–i) also showed the hierarchical structure of the modified layer. The element distribution of the modified membrane from top to bottom was Co, Fe, Zr, and Al, while O was presented on the whole cross-section. This was mainly due to the higher reaction constant of Fe^{3+} with OH^- (−13.1 and −18.8, respectively), so Fe_2O_3 deposited on the membrane surface first [30], and a bilayer structure of Co_3O_4 and Fe_2O_3 was formed.

The Raman spectroscopy of the membranes was shown in Fig. 16 (a). The four peaks at 181 cm^{-1}, 194 cm^{-1}, 335 cm^{-1}, and 476 cm^{-1} were the active vibrational peaks of ZrO_2 [38] as the main material of substrate membrane. The characteristic peaks at 488 cm^{-1},

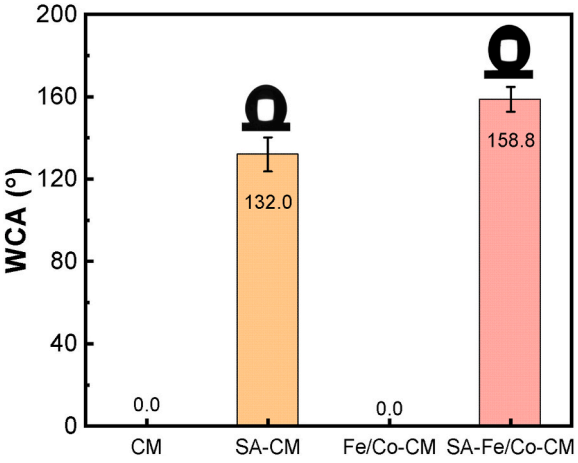

Fig. 17. Water contact angle of different membranes.

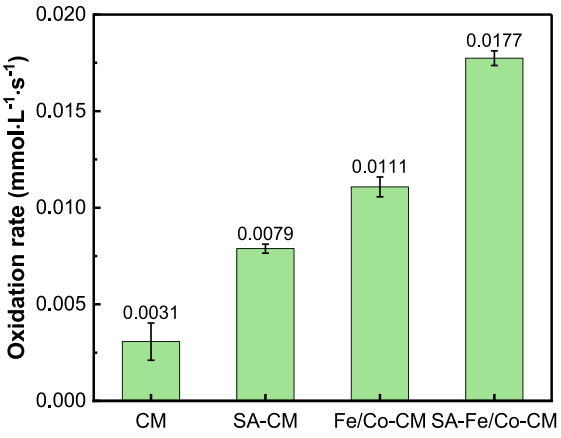

Fig. 18. Oxidation rate of the different membranes.

525 cm^{-1} and 623 cm^{-1} and 693 cm^{-1} corresponded to Co_3O_4 were observed on the Fe/Co-CM and SA-Fe/Co-CM membranes [39], while no peak related to Fe_2O_3 and ZrO_2 were presented. It was revealed that Fe_2O_3 was in the second layer and Co_3O_4 was dominant substance on the surface.

The functional groups on the membrane surface were also determined by FTIR (Fig. 16 (b)). The broad peaks at 3340 cm^{-1} were corresponded to the stretching vibrations of –OH. The peaks at 2927 cm^{-1}, 2857 cm^{-1} and 1740 cm^{-1} were corresponded to the stretching vibrations of $–CH_3$, $–CH_2$ and $-COO^-$[43] respectively, indicating that stearic acid has been successfully incorporated on the membrane surface. As shown in Fig. 17, The contact angle of SA-CM and SA-Fe/Co-CM were 132° ± 8.3° and 158.8° ± 6.01°, respectively, while the ones of CM and Fe/Co-CM membranes were close to 0°. Therefore, the modification of stearic acid improved the hydrophobicity of the membranes attributed to the long carbon chains of stearic acid.

The sulfite reaction rates of CM, SA-CM, Fe/Co-CM and SA-Fe/Co-CM membranes were shown in Fig. 18. It was presented that the reaction rate was increased from 0.0031 mmol L^{-1} s^{-1} to 0.0079 mmol L^{-1} s^{-1} after hydrophobic modification by SA. It was mainly because the air film between the hydrophobic membrane surface and the aqueous solution could reduce the oxygen transfer resistance and the size of the generated bubbles [44], which will lead to higher mass transfer efficiency and longer residence time in water, which increasing the dissolved oxygen and generating hydroxyl radicals with strong oxidizing ability [45]. Thus, the oxidation of sulfites was sped up. The increase in oxidation rate of Fe/Co-CM compared to CM demonstrated the catalytic role of Fe/Co oxides in the reaction process, while the oxidation rate of SA-Fe/Co-CM membranes was enhanced by 5.8 times than that of CM membranes. On the one hand, the loading of oxides produced a secondary rough structure and abundant hydroxyl groups on the membrane surface, which led to a stronger hydrophobicity [46]. On the other hand, the hydrophobic surface could reduce the resistance of gas transport and facilitate the exposure of the catalytic active sites [47]. The reaction rate for the Co-loaded membrane and the Fe-loaded membrane were both lower than those for the modified membranes produced by mixed Fe/Co oxides. The results indicated that the catalytic effect of the modified membranes was enhanced by the simultaneous development of Fe/Co oxides onto the membranes. The findings demonstrated that the method of bimetallic catalyst loading in conjunction with hydrophobic modification enhanced the catalytic

effect of ceramic membranes. The bimetal has a stronger catalytic effect, and the hydrophobic layer assures catalyst activity while lowering mass transfer resistance.

4. Conclusion

A series of superhydrophobic ceramic membranes loaded with Fe_2O_3 and Co_3O_4 were fabricated through hydrothermal method and hydrophobic modification. These two oxides presented an approximate double-layer distribution on the membrane surface. The Co_3O_4 in upper layer was the main catalyst, and Fe_2O_3 in the lower layer could improve stability and catalytic performance of Co. The hierarchical structure of Fe/Co oxide was benefit for increasing the dispersion of catalytic active component, enhancing the catalytic performance, decreasing the leaching of ions, and reducing the environment risk. Its catalytic performance was decreased with the increasing of Fe/Co ratio and declined after an initial rise with the increase of urea and CTAB. The sulfite oxidation rate with the SA-Fe/Co-CM membrane was 5.8 times higher than the one with original membrane. The catalytic oxidation rate would keep constant after 5 times experiments with a decrease of 15 %, which was smaller compared to that of single metal sample. This work will provide a new method for the development of sulfite oxidation catalyst and the reduce of the catalyst costs and potential environmental toxicity.

Data availability statement

No data associated in this article has been deposited into a publicly available repository. The data that support the findings of this study are available from the corresponding author, [Jie Liu], on request.

CRediT authorship contribution statement

Lijuan Feng: Writing – original draft, Investigation, Data curation. **Jie Liu:** Writing – review & editing, Supervision, Resources, Project administration, Methodology, Funding acquisition, Conceptualization. **Shizhao Wang:** Writing – review & editing, Formal analysis. **Yingying Zhao:** Writing – review & editing. **Fei Li:** Formal analysis. **Xiaofu Guo:** Visualization. **Junsheng Yuan:** Resources, Funding acquisition.

Declaration of competing interest

The authors declare that they have no known competing financial interests or personal relationships that could have appeared to influence the work reported in this paper.

Acknowledgement

This work was supported by Natural Science Foundation of Hebei Province, China (B2022202050) and Key Research & Development Plan of Hebei Province, China (22373703D).

References

[1] A. Gupta, S. Ibrahim, A. Al Shoaibi, Advances in sulfur chemistry for treatment of acid gases, Prog. Energy Combust. Sci. 54 (2016) 65–92.
[2] M. Al-Jahdali, A.B. Bisher, Sulfur dioxide (SO_2) accumulation in soil and plant's leaves around an oil refinery: a case study from Saudi Arabia, Am. J. Environ. Sci. 4 (1) (2008) 84–88.
[3] X.K. Li, J.R. Han, Y. Liu, et al., Summary of research progress on industrial flue gas desulfurization technology, Sep. Purif. Technol. 281 (2022) 119849.
[4] J. Zhu, S.C. Ye, J. Bai, et al., A concise algorithm for calculating absorption height in spray tower for wet limestone–gypsum flue gas desulfurization, Fuel Process. Technol. 129 (2015) 15–23.
[5] J.J. Bao, L.J. Yang, W.D. Sun, et al., Removal of fine particles by heterogeneous condensation in the double-alkali desulfurization process, Chem. Eng. Process: Process Intensif. 50 (8) (2011) 828–835.
[6] R. del Valle-Zermeño, J. Formosa, J.A. Aparicio, et al., Transposition of wet flue gas desulfurization using MgO by-products: from laboratory discontinuous batch reactor to pilot scrubber, Fuel Process. Technol. 138 (2015) 30–36.
[7] X. Gao, H.L. Ding, Z. Du, et al., Gas–liquid absorption reaction between $(NH_4)_2SO_3$ solution and SO_2 for ammonia-based wet flue gas desulfurization, Appl. Energy 87 (8) (2010) 2647–2651.
[8] K. Oikawa, C. Yongsiri, K. Takeda, et al., Seawater flue gas desulfurization: its technical implications and performance results, Environ. Prog. 22 (1) (2003) 67–73.
[9] Z.G. Shen, X. Chen, M. Tong, et al., Studies on magnesium-based wet flue gas desulfurization process with oxidation inhibition of the byproduct, Fuel 105 (2013) 578–584.
[10] M.M. Dai, J. Liu, Z.Y. Ji, et al., Fabrication of superhydrophobic & catalytic bifunctional MnO_2@ Al_2O_3 composite ceramic membrane for oxidation of desulfurization waste solution, Colloids Surf. A Physicochem. Eng. Asp. 635 (2022) 128067.
[11] Y.Y. Yang, C.M. Zhu, Y. Zhang, et al., Construction of Co_3O_4/Fe_2O_3 nanosheets on nickel foam as efficient electrocatalyst for the oxygen evolution reaction, J. Phys. Chem. Solid. 148 (2021) 109680.
[12] J. Liu, S. Lu, L.D. Wang, et al., Co-site substitution by Mn supported on biomass-derived active carbon for enhancing magnesia desulfurization, J. Hazard Mater. 365 (2019) 531–537.
[13] L.D. Wang, T.Y. Qi, S.Y. Wu, et al., A green and robust solid catalyst facilitating the magnesium sulfite oxidation in the magnesia desulfurization process, J. Mater. Chem. A 5 (17) (2017) 8018–8028.
[14] Q.T. Sun, B.D. Xu, J. Yang, et al., Layered oxides supported Co-Fe bimetal catalyst for carbamazepine degradation via the catalytic activation of peroxymonosulfate, Chem. Eng. J. 400 (2020) 125899.
[15] R.X. Zhang, Z.C. Hu, T.Y. Ning, et al., Heterophase stimulated active species evolution in iron/cobalt sulfide nanocomposites for oxygen evolution, Colloids Surf. A Physicochem. Eng. Asp. (2022) 129181.

[16] K.D. Zhi, C. Yang, Y. Zheng, et al., Enhanced electro-fenton degradation of ciprofloxacin by membrane aeration, Ind. Eng. Chem. Res. (2022) 8141–8148.
[17] M. Takahashi, K. Chiba, P. Li, Free-radical generation from collapsing microbubbles in the absence of a dynamic stimulus, J. Phys. Chem. B 111 (6) (2007) 1343–1347.
[18] D.W. Lu, H. Bai, F.G. Kong, et al., Recent advances in membrane aerated biofilm reactors, Crit. Rev. Environ. Sci. Technol. 51 (7) (2021) 649–703.
[19] J.W. Hou, G.X. Dong, B.W. Xiao, et al., Preparation of titania based biocatalytic nanoparticles and membranes for CO_2 conversion, J. Mater. Chem. A 3 (7) (2015) 3332–3342.
[20] S. Kumar, J. Cho, I. Moon, International Journal of Greenhouse Gas Control Ionic liquid-amine blends and CO_2 BOLs: prospective solvents for natural gas sweetening and CO_2 capture technology—a review, Int. J. Greenh. Gas Control 20 (2014) 87–116.
[21] X.L. Li, H. Jiang, M.M. Hou, et al., Enhanced phenol hydrogenation for cyclohexanone production by membrane dispersion, Chem. Eng. J. 386 (2020) 120744.
[22] M. Peng, Y. Liu, H. Jiang, et al., Enhanced catalytic properties of Pd nanoparticles by their deposition on ZnO-coated ceramic membranes, RSC Adv. 6 (3) (2016) 2087–2095.
[23] Y.Y. Chu, H.Z. Su, C. Liu, et al., Fabrication of sandwich-like super-hydrophobic cathode for the electro-Fenton degradation of cefepime: H_2O_2 electro-generation, degradation performance, pathway and biodegradability improvement, Chemosphere 286 (2022) 131669.
[24] W.H. Gu, B. Quan, X.H. Liang, et al., Composition and structure design of Co_3O_4 nanowires network by nickel foam with effective electromagnetic performance in C and X band, ACS Sustain. Chem. Eng. 7 (5) (2019) 5543–5552.
[25] M.H. Su, C. He, K.M. Shih, Facile synthesis of morphology and size-controlled α-Fe_2O_3 and Fe_3O_4 nano-and microstructures by hydrothermal/solvothermal process: the roles of reaction medium and urea dose, Ceram. Int. 42 (13) (2016) 14793–14804.
[26] H. Meng, J.T. Bi, J. Liu, et al., MnO_2-Functionalized hydrophobic ceramic membrane for sulfite oxidation, ACS Appl. Nano Mater. 6 (8) (2023) 6772–6783.
[27] L. Pérez-Pérez, A. Báez-Rodríguez, L. García-González, et al., Nanopores and nanosheets of α-Fe_2O_3 synthetized by electrochemical anodization and analysed by Raman spectroscopy, MRS Advances 4 (53) (2019) 2863–2871.
[28] I. Lorite, J. Romero, J. Fernández, Effects of the agglomeration state on the Raman properties of Co_3O_4 nanoparticles, J. Raman Spectrosc. 43 (10) (2012) 1443–1448.
[29] J.F. Xu, W. Ji, Z.X. Shen, et al., Raman spectra of CuO nanocrystals, J. Raman Spectrosc. 30 (5) (1999) 413–415.
[30] D.W. Barnum, Hydrolysis of cations. Formation constants and standard free energies of formation of hydroxy complexes, Inorg. Chem. 22 (16) (1983) 2297–2305.
[31] P.K. Katkar, S.J. Marje, S.B. Kale, et al., Synthesis of hydrous cobalt phosphate electro-catalysts by a facile hydrothermal method for enhanced oxygen evolution reaction: effect of urea variation, CrystEngComm 21 (5) (2019) 884–893.
[32] Dhas C. Ravi, R. Venkatesh, K. Jothivenkatachalam, et al., Visible light driven photocatalytic degradation of Rhodamine B and Direct Red using cobalt oxide nanoparticles, Ceram. Int. 41 (8) (2015) 9301–9313.
[33] Z.Y. Liu, Q.Y. Wang, W. Rong, et al., CTAB assisted hydrothermal preparation of $Bi_2WO_6WO_3$ nanosheets on TiO_2 nanotube arrays for photoelectrocatalytic applications, Sep. Purif. Technol. 200 (2018) 191–197.
[34] N.B. Velhal, T.H. Yun, J. Ahn, et al., Tailoring cobalt oxide nanostructures for stable and high-performance energy storage applications, Ceram. Int. 49 (3) (2023) 4889–4897.
[35] K. Kaviyarasu, E. Manikandan, Z. Nuru, et al., Investigation on the structural properties of CeO_2 nanofibers via CTAB surfactant, Mater. Lett. 160 (2015) 61–63.
[36] Y.Q. Li, T.M. Liu, T.M. Li, et al., Hydrothermal fabrication of controlled morphologies of MoO_3 with CTAB: structure and growth, Mater. Lett. 140 (2015) 48–50.
[37] A.N. Naveen, S. Selladurai, Tailoring structural, optical and magnetic properties of spinel type cobalt oxide (Co_3O_4) by manganese doping, Phys. B Condens. Matter 457 (2015) 251–262.
[38] Y.K. Penke, G. Anantharaman, J. Ramkumar, et al., Aluminum substituted cobalt ferrite (Co−Al−Fe) nano adsorbent for arsenic adsorption in aqueous systems and detailed redox behavior study with XPS, ACS Appl. Mater. Interfaces 9 (13) (2017) 11587–11598.
[39] J. Liu, J. Ke, Y. Li, et al., Co_3O_4 quantum dots/TiO_2 nanobelt hybrids for highly efficient photocatalytic overall water splitting, Appl. Catal. B Environ. 236 (2018) 396–403.
[40] Z.M. Fang, L. Xing, Y.B. Liu, et al., Ternary heterojunction stabilized photocatalyst of Co-TiO_2/g-C_3N_4 in boosting sulfite oxidation during wet desulfurization, Appl. Surf. Sci. 551 (2021) 149478.
[41] T. Choudhury, S. Saied, J. Sullivan, et al., Reduction of oxides of iron, cobalt, titanium and niobium by low-energy ion bombardment, J. Phys. Appl. Phys. 22 (8) (1989) 1185.
[42] S. Saha, B. Dutta, M. Ghosh, et al., Adsorption of 4-mercapto pyridine with gold nanoparticles embedded in the Langmuir–blodgett film matrix of stearic acid: SERS, XPS studies aided by born–oppenheimer on the fly dynamics, time–resolved wavelet transform theory, and DFT, ACS Omega 7 (32) (2022) 27818–27830.
[43] A. Benkaddour, E.C. Demir, N.C. Jankovic, et al., A hydrophobic coating on cellulose nanocrystals improves the mechanical properties of polyamide-6 nanocomposites, J. Compos. Mater. 56 (11) (2022) 1775–1788.
[44] A.K.A. Ahmed, C. Sun, L. Hua, et al., Generation of nanobubbles by ceramic membrane filters: the dependence of bubble size and zeta potential on surface coating, pore size and injected gas pressure, Chemosphere 203 (2018) 327–335.
[45] M. Yao, J. Bai, Y.H. Chang, et al., Effects of air flowrate distribution and benzene removal in heterogeneous porous media during air sparging remediation, J. Hazard Mater. 398 (2020) 122866.
[46] L.B. Feng, H.X. Zhang, P.Z. Mao, et al., Superhydrophobic alumina surface based on stearic acid modification, Appl. Surf. Sci. 257 (9) (2011) 3959–3963.
[47] G.D. Zhang, X.S. Huang, Z.C. Tang, Enhancing water resistance of a Mn-based catalyst for low temperature selective catalytic reduction reaction by modifying super hydrophobic layers, ACS Appl. Mater. Interfaces 11 (40) (2019) 36598–36606.